Numerical Modelling of Thermal Weakening Effect on Compressive Strength of Concrete

Timo Saksala[a)], Reijo Kouhia[b)]

Tampere University, Tampere, Finland

[a)]Corresponding author: timo.saksala@tuni.fi
[b)]reijo.kouhia@tuni.fi

Abstract. Concrete strength reduces considerably at elevated temperatures. In the present study, this weakening effect is numerically modelled with the embedded discontinuity finite elements approach. Concrete material is modelled mesoscopically as an aggregate-mortar bi-phasic structure made of Portland cement and granite. Initial crack populations are applied to the cement matrix to add randomness. The concrete material is linear elastic until violation of the Rankine criterion upon which a crack, with a normal parallel to the first principal direction, is introduced into a constant strain triangle element. This fracture model appears to replicate the salient features of concrete fracture in compression. The thermally induced cracking is simulated by solving the underlying thermo-mechanical problem with an explicit staggered scheme using mass scaling to increase the critical time step. Numerical 2D simulations of concrete under uniaxial compression demonstrate that the present method predicts the thermal weakening effect with an engineering accuracy.

INTRODUCTION

As a major construction material, concrete is often exposed to high temperatures (e.g. during fire), which lead to a degradation of concrete strength [1-4]. Therefore, understanding the concrete fracture processes under thermal and thermo-mechanical loading conditions is of substantial practical importance in structural engineering. Considerable number of numerical studies has thus been devoted to modelling of the concrete behavior under elevated temperatures, see [5-7] for just a few examples.

Ignoring the chemical and hydrothermal effects for simplicity, the thermal weakening of concrete can be traced to the heterogeneity of the cement matrix-rocky aggregate mesostructure. More precisely, is assumed here that the elastic and thermal expansion mismatch between the cement and the aggregates generates thermal stresses, which in turn leads to cracking of the concrete material. Thereby, the explicit description of this bi-phasic concrete mesostructure cannot be ignored, as is done in the usual homogenization techniques. Moreover, the aggregates introduce various fracture toughening mechanisms, such as crack stopping, redirection and branching [8].

This paper presents a modelling approach to predict the thermal weakening effect on the compressive strength of concrete with rough aggregates. The model, originally presented by Saksala [7], is based on the embedded discontinuity finite elements with a Rankine criterion to introduce a crack in a linear triangle element. A staggered explicit scheme is employed to solve the global FE discretized thermo-mechanical problem in time. The model performance is tested in 2D simulations of concrete under uniaxial compression at room and elevated temperatures.

NUMERICAL APPROACH

Concrete fracture model

Concrete fracture is described by the embedded discontinuity finite elements. For a constant strain triangle (CST) element with a strong discontinuity (crack) illustrated in Fig. 1a, the displacement and strain fields are

$$\mathbf{u} = N_i \mathbf{u}_i^e + (H_{\Gamma_d} - \varphi)\boldsymbol{\alpha}_d, \quad \boldsymbol{\varepsilon} = \nabla N_i \otimes \mathbf{u}_i^e - \nabla\varphi \otimes \boldsymbol{\alpha}_d \tag{1}$$

$$\nabla\varphi = \arg\left(\max_{k=1,2} \frac{\left|\Sigma_{i=1}^{k} \nabla N_i \cdot \mathbf{n}_\mathrm{d}\right|}{\left\|\Sigma_{i=1}^{k} \nabla N_i\right\|}\right) \tag{2}$$

where N_i and $\mathbf{u}_i^e$ are the standard interpolation functions and nodal displacements (i = 1,2,3 with summation on repeated indices), respectively, and $\boldsymbol{\alpha}_d$ is the displacement jump. Moreover, H_{Γ_d} is the Heaviside function at the discontinuity. Furthermore, in arriving to the expression for the strain $\boldsymbol{\varepsilon}$, it was assumed that $\nabla\boldsymbol{\alpha}_d \equiv \mathbf{0}$, i.e. the displacement jump is elementwise constant. In Eq. (1), φ is a function that restricts the effect of the displacement jump within the corresponding finite element so that the essential boundary conditions remain unaffected. It is chosen, from among the possible combinations of the shape functions by criterion (2), so that its gradient is as parallel as possible to the crack normal $\mathbf{n}_d$.

Next, the strong traction balance over the discontinuity, imposed in the present approach, along with the constitutive equation are specified as

$$\mathbf{t}_{\Gamma_d} = \boldsymbol{\sigma} \cdot \mathbf{n}_d \tag{3}$$

$$\boldsymbol{\sigma} = \mathbf{E}\colon (\hat{\boldsymbol{\varepsilon}} - (\nabla\varphi(\mathbf{x}) \otimes \boldsymbol{\alpha}_d)^{sym} - \boldsymbol{\varepsilon}_\theta), \;\; \boldsymbol{\varepsilon}_\theta = \alpha\Delta\theta\mathbf{I} \tag{4}$$

In Eq. (3), $\boldsymbol{\sigma}$ is the stress tensor, and $\mathbf{t}_{\Gamma_d}$ is the traction vector, while in Eq. (4), $\mathbf{E}$ is the elasticity tensor, $\hat{\boldsymbol{\varepsilon}} = (\nabla N_i \otimes \mathbf{u}_i^e)^{sym}$, and $\boldsymbol{\varepsilon}_\theta$ is the thermal strain with $\alpha, \Delta\theta, \mathbf{I}$ being the thermal expansion coefficient, temperature increment and the second order identity tensor, respectively.

Finally, a bi-surface, plasticity inspired model for solving the displacement jump vector and the traction, as well as to control the softening behaviour at the discontinuity is specified. The components of this model are

$$\phi_t(\mathbf{t}_{\Gamma_d}, \kappa, \dot{\kappa}) = \mathbf{n} \cdot \mathbf{t}_{\Gamma_d} - (\sigma_t + q(\kappa, \dot{\kappa})), \quad \phi_s(\mathbf{t}_{\Gamma_d}, \kappa, \dot{\kappa}) = |\mathbf{m} \cdot \mathbf{t}_{\Gamma_d}| - (\sigma_s + \frac{\sigma_s}{\sigma_t} q(\kappa, \dot{\kappa})) \tag{5}$$

$$\dot{\boldsymbol{\alpha}}_d = \dot{\boldsymbol{\alpha}}_I + \dot{\boldsymbol{\alpha}}_{\mathrm{II}} = \dot{\lambda}_t \frac{\partial\phi_t}{\partial\mathbf{t}_{\Gamma_d}} + \dot{\lambda}_s \frac{\partial\phi_s}{\partial\mathbf{t}_{\Gamma_d}}, \quad \dot{\mathbf{t}}_{\Gamma_d} = -\mathbf{E}\colon (\nabla\varphi \otimes \dot{\boldsymbol{\alpha}}_d) \cdot \mathbf{n}, \quad \dot{\kappa} = -\dot{\lambda}_t \frac{\partial\phi_t}{\partial q} - \dot{\lambda}_s \frac{\partial\phi_s}{\partial q} \tag{6}$$

$$q = h\kappa + s\dot{\kappa}, \quad h = -g\sigma_t \exp(-g\kappa), \quad \dot{\lambda}_i \geq 0, \quad \phi_i \leq 0, \quad \dot{\lambda}_i\phi_i = 0, \quad i = \mathrm{t,s} \tag{7}$$

In Eq. (5), ϕ_t and ϕ_s are the tension (mode I) and shear (mode II) loading functions, respectively, $\kappa, \dot{\kappa}$ are the internal variable and its rate, $\mathbf{m}$ is the crack tangent vector, and σ_t and σ_s are elastic limits in tension and shear, respectively. Equation (6) specifies the evolution equations for $\boldsymbol{\alpha}_\mathrm{I}$, $\boldsymbol{\alpha}_\mathrm{II}$, i.e. the mode I and II crack opening vectors, and for κ in terms of the mode I and II opening increments, $\dot{\lambda}_t$, $\dot{\lambda}_s$, respectively. In Eq. (7), h is the softening modulus, and s is the constant viscosity modulus. The softening slope parameter g is defined by the mode I fracture energy G_Ic by $g = \sigma_t / G_\mathrm{Ic}$. Equation (7) has also the consistency conditions, which enable the solution of this local problem using the computational plasticity methods.

The material behaviour is linear elastic upon violation of Rankine criterion. When this happens, a discontinuity is embedded in an element with a (fixed) normal parallel to the first principal direction. However, once a crack is introduced, it can fail in both shear and tensile mode, as governed by the model above.

Solution of global thermo-mechanical problem

The governing initial/boundary value problem in the strong form can be written as

$$\rho\ddot{\mathbf{u}} = \nabla \cdot \boldsymbol{\sigma} + \mathbf{b} \tag{8}$$

$$\rho c\dot{\theta} = -\nabla \cdot \mathbf{q} + Q_\mathrm{mech} \tag{9}$$

where ρ and c are the density and the specific heat capacity of the material, and the rest of the symbols are as follows: $\dot{\theta}$ is the rate of change of temperature; $\ddot{\mathbf{u}}$ is the acceleration vector; $\mathbf{b}$ is the volume force; $\mathbf{q}$ is the heat flux vector related to temperature gradient $\nabla\theta$ and the conductivity k by the Fourier's law $\mathbf{q} = -k\nabla\theta$.

In Eq. (9), Q_{mech} expresses the mechanical heat production through dissipation and strain rate. These sources of heat are, being insignificant compared to the external heat influx, ignored, i.e. $Q_{\mathrm{mech}} \equiv 0$. The finite element discretized form of the local thermo-mechanical problem can be derived through standard steps exploiting the principle of virtual work. In the present paper, the global problem is solved explicitly in time leading to following equations for the new temperature and mechanical response:

$$\mathbf{C}_\theta \boldsymbol{\theta}_{t+\Delta t} = \mathbf{C}_\theta \boldsymbol{\theta}_t + \Delta t(\mathbf{f}_{\theta,t} - \mathbf{K}_\theta \boldsymbol{\theta}_t) \rightarrow \boldsymbol{\theta}_{t+\Delta t} \tag{10}$$

$$\mathbf{M}\ddot{\mathbf{u}}_t + \mathbf{f}_{\mathrm{int},t}(\mathbf{u}_t, \dot{\mathbf{u}}_t, \boldsymbol{\theta}_t) = \mathbf{f}_{\mathrm{ext},t} \rightarrow \ddot{\mathbf{u}}_t \tag{11}$$

$$\dot{\mathbf{u}}_{t+\Delta t} = \dot{\mathbf{u}}_t + \Delta t \ddot{\mathbf{u}}_t \tag{12}$$

$$\mathbf{u}_{t+\Delta t} = \mathbf{u}_t + \Delta t \dot{\mathbf{u}}_{t+\Delta t} \tag{13}$$

where

$$\mathbf{f}_{\mathrm{int}} = \mathbf{A}_{\mathrm{e}=1}^{\mathrm{N_e}} \int_{V_\mathrm{e}} \mathbf{B}_\mathrm{e}^\mathrm{T} \boldsymbol{\sigma}_\mathrm{e}(\mathbf{u}_t, \dot{\mathbf{u}}_t, \boldsymbol{\theta}_t) \mathrm{d}V, \quad \mathbf{M} = \mathbf{A}_{\mathrm{e}=1}^{\mathrm{N_e}} \int_{V_\mathrm{e}} \rho \mathbf{N}_\mathrm{e}{}^\mathrm{T} \mathbf{N}_\mathrm{e} \, \mathrm{d}V \tag{14}$$

$$\mathbf{C}_\theta = \mathbf{A}_{\mathrm{e}=1}^{\mathrm{N_e}} \int_{V_\mathrm{e}} \rho c \mathbf{N}_\theta^{\mathrm{e,T}} \mathbf{N}_\theta^\mathrm{e} \mathrm{d}V, \quad \mathbf{K}_\theta = \mathbf{A}_{\mathrm{e}=1}^{\mathrm{N_e}} \int_{V_\mathrm{e}} k \mathbf{B}_\theta^{\mathrm{e,T}} \mathbf{B}_\theta^\mathrm{e} \mathrm{d}V \tag{15}$$

$$\mathbf{f}_\theta = \mathbf{A}_{\mathrm{e}=1}^{\mathrm{N_e}} \int_{V_\mathrm{e}} Q_{int} \mathbf{N}_\theta^{\mathrm{e,T}} \, \mathrm{d}V \tag{16}$$

In these equations, $\mathbf{M}$ is the consistent mass matrix (to be lumped by the row sum technique); $\mathbf{C}$ is capacity matrix (to be lumped by the row sum technique), $\mathbf{K}_\theta$ is the conductivity matrix; $\mathbf{f}_{\mathrm{ext}}$ is the external force vector; $\mathbf{f}_{\mathrm{int}}$ is the internal force vector; $\mathbf{f}_\theta$ is the vector of thermal loading with Q_{int} being the volumetric heating magnitude (flux); Δt is the time step; $\mathbf{A}$ is the standard finite element assembly operator; $\mathbf{B}_\mathrm{e}$ is the kinematic matrix (mapping the nodal displacement into element strains); $\boldsymbol{\theta}$ is the nodal temperature vector; $\mathbf{N}_\theta$ and $\mathbf{N}_\mathrm{e}$ are the temperature and displacement interpolation matrices (same interpolation functions are used in both); $\mathbf{B}_\theta$ is the gradient of $\mathbf{N}_\theta$.

Concrete mesoscale description

Concrete is described as a two-phase material with explicit aggregates in a cement matrix. The aggregates are taken to be convex polygons with random sizes and locations. The resulting mortar-aggregate structure is meshed with the ordinary CST elements. Concrete contains inherent microcrack populations induced, e.g. by hydration processes. These cracks have, expectedly, a non-negligible influence on the concrete failure processes. They are therefore modelled here explicitly.

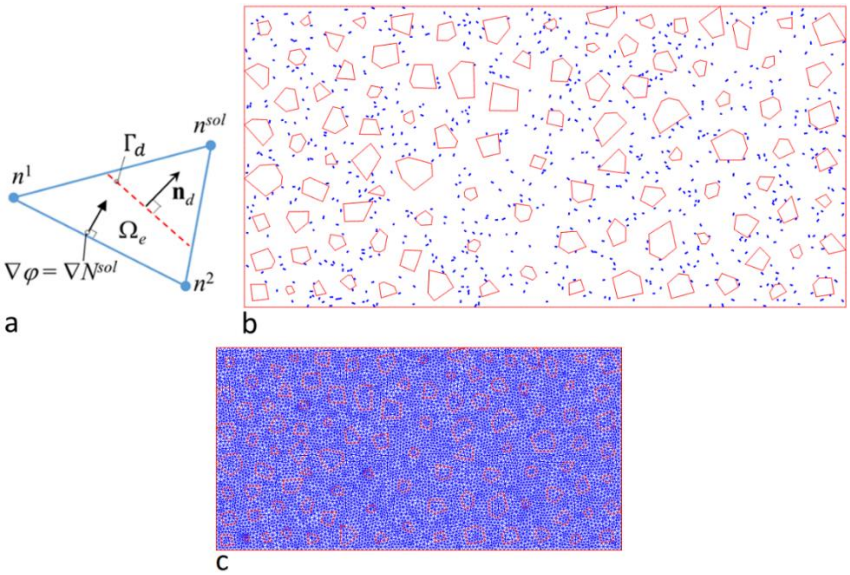

FIGURE 1. (a) Linear triangle element with a discontinuity; (b) Numerical concrete (dimensions: 100mm×50mm); (c) Finite element mesh (17330 elements).

Figure 1b shows the numerical concrete mesostructure with the aggregates represented by 100 polygons of different shapes and sizes. The blue lines (719 in total) represent the inherent microcrack population, modelled as pre-embedded discontinuities with random orientations (i.e. their alignment angle is uniformly distributed between $-\pi/2$ and $\pi/2$). It is assumed that only the cement matrix contains initial cracks. Moreover, the tensile and shear strengths of the initial cracks are set to close to zero so that they can open without any resistance. Figure 1c shows the finite element mesh with 17330 triangle elements.

NUMERICAL EXAMPLES

A representative numerical example demonstrating the performance of the present approach is presented here. More specifically, uniaxial compression test is carried out on the numerical concrete in Fig. 1 before and after heat treatment. First, the material properties and model parameters are specified in Table 1.

TABLE 1. Model parameter values for simulations

Property/Parameter	Mortar Value	Aggregates Value	Unit
E (Young's modulus)	27.5	50	GPa
ν (Poisson's ratio)	0.2	0.2	
ρ (Material density)	2400	2400	kg/m^3
σ_t (Tensile strength)	3.5	8	MPa
σ_s (Shear strength)	7	25	MPa
G_{Ic} (fracture energy)	20	40	N/m
s (Viscosity)	0.005	0.005	MPa·s/m
c (Specific heat capacity)	731	731	J/kg·K
k (Conductivity)	1.4	2.85	W/m·K
α (Thermal exp. coeff.)	11E-6	8E-6	K^{-1}

The mechanical and thermal properties of the mortar are the averages of the range given for Portland cement on the website www.engineeringtoolbox.com, while the aggregate values represent generic granite. The value of viscosity is set low enough to not cause any strain rate effects. At this preliminary stage of developments, the material properties are taken as temperature independent. This is a plausible assumption with respect to strength and stiffness, which are measured for a laboratory sample level behavior, not at the material point level. It would be somewhat circular reasoning to feed the laboratory test data as a model input at the material point level constitutive description and then predict that same data in the numerical simulations.

Heat treatment simulation

In the experiments [1-4], the concrete samples are slowly heated (~ 1-2 h) in an oven to a target temperature after which they are left to naturally cool down to the room temperature. The compression test is then carried out on the heat-treated samples at the room temperature.

Uniform heating up to 500 °C is carried out on the numerical concrete (Fig. 1). Mass scaling, enabled by the non-inertial nature of slow heating, is applied to the mechanical equation (11) using 10000-fold density to increase the critical time step of the explicit time stepping. Despite the mass scaling, which increases the critical time step 100-fold (being then 4.6×10^{-6} s), a practical simulation time requires applying volumetric heating with Q_{int} = 1 GW/m^3 (Eq. (16)) at each node of mesh to secure a homogenous temperature field in the concrete sample. With this extreme intensity, the target temperature (500 °C) is reached in a physical time of 0.84 s (requiring some 182000 time steps taking ≈1 day of CPU time with the present Matlab implementation). The simulation results are shown in Fig. 2.

This heating induces cracks mostly in the aggregates and to their immediate vicinity, as observed in Fig. 2c. The orientation of the cracks in the narrow strip surrounding the aggregates are parallel to the aggregate edges. This reflects the fact that the principal stress directions at the elements therein are orthogonal to the aggregate edges. As the tensile

strength of the cement is only 3.5 MPa, the cracks in the elements surrounding the aggregates also open more than the cracks inside the aggregates, as observed in Fig. 2b.

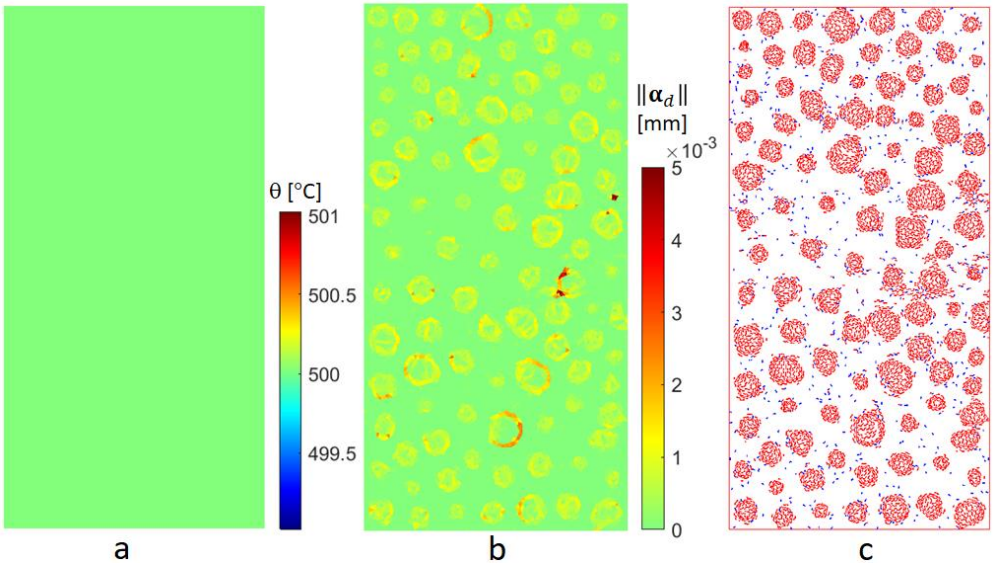

FIGURE 2. (a) Temperature distribution at the end of heating; (b) Crack opening magnitude at the end of heating; (c) Thermally induced cracks at the end of heating.

Compression tests

Now, the compression tests are performed on the numerical concrete in Fig. 1 in its intact state and on the heat-treated concrete. For this end, the cracks, and their residual strengths (the values of q reached in the end of heating) are set as an initial state for the numerical compression test on the heat-treated concrete. A constant velocity boundary condition is applied at one of the short edges of the sample while the other edge is simply supported. The simulation results are shown in Fig. 3.

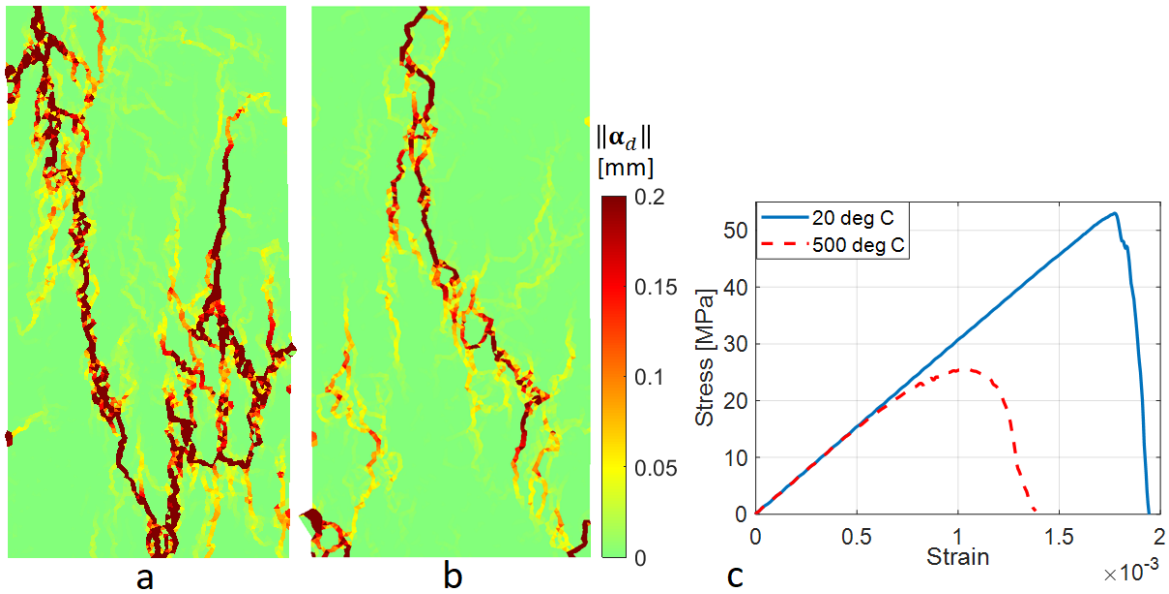

FIGURE 3. (a) Failure mode in terms of crack opening magnitude for the intact concrete; (b) Failure mode in terms of crack opening magnitude for the heat-treated concrete; (c) Corresponding average stress-strain curves.

The predicted failure mode for the intact sample shows typical features of the axial splitting mode observed for concrete [1-4]. The heat-treated sample naturally attest differing details due to the initial crack distribution. The corresponding compressive strengths are 53 MPa for the intact and 25.6 MPa for heated sample. The curve for the intact concrete has features of a brittle behaviour with an almost linear pre-peak and very steep post-peak parts. In contrast, the heat-treated sample has a clear pre-peak nonlinear part due to the initial cracks, which start to open well before the peak stress is reached.

As to the thermal weakening effect, the normalized strength at 500 °C is 0.48 (25.6/53). The experimental scatter is quite large and depends on the aggregate type used. For example, according to the data for several concretes collected by Bastami et al. [2], the experimental data is scattered, respectively, between values [0.41, 0.88] and [0.58, 0.88] for silicious and carbonate aggregates at 500 °C. Therefore, the present prediction is barely within the scatter for silicious aggregates.

CONCLUSION

This paper presented a numerical approach based on the embedded discontinuity finite elements and an explicit time stepping scheme to solve the global discretized thermo-mechanical problem. The global solution scheme employs extreme mass scaling with lumped mass and capacity matrices formulation, as well as volume heating, which makes the method feasible for simulation of slow heating problem due to its non-inertial nature.

The method predicted the correct failure mode of concrete under uniaxial compression. However, slight overprediction of the thermal weakening at 500 °C was observed. Given that the constitutive model is temperature independent at this initial stage of developments, its performance could be substantially improved if the thermal expansion coefficient, of both the cement matrix and the aggregates, is made temperature dependent, as it truly is in reality. This topic will be covered in the future studies of the method.

REFERENCES

1. A. El-Zohairy, H. Hammontree, E. Oh and P. Moler, *Materials* **13**, 2801 (2020).
2. M. Bastami, F. Aslani and M. Esmaeilnia Omran, *IJCE*, **8**, 337-351 (2010), http://ijce.iust.ac.ir/article-1-185-en.html.
3. V. Kodur, *ISRN Civil Engineering*, Volume 2014, Article ID 468510, http://dx.doi.org/10.1155/2014/468510.
4. M. M. Rafi, T. Aziz, and S. H. Lodi, *J. Struct. Fire Eng.* **8**, 418-439 (2017).
5. P. Grassl and C. Pearce, *J. Eng. Mech.*, **136**, 322-328 (2010).
6. A. Caggiano and E. Guillermo, *Comput. Methods Appl. Mech. Engng*. **289**, 498-516 (2015).
7. T. Saksala, *Eng. Fract. Mech.* **201**, 282-297 (2018).
8. E.N. Landis and J.E. Bolander, *Journal of Physics D: Applied Physics* **42**, 214002 (2009).